Hyperfine Interactions 123/124 (1999) 633–663

Perturbation of nuclear excitons by ultrasound

G.V. Smirnov [a] and W. Potzel [b]

[a] *Russian Research Center "Kurchatov Institute", Moscow 123182, Russia*
[b] *Physik-Department E15, Technische Universität München, D-85747 Garching, Germany*

The coherent decay of a nuclear exciton created by synchrotron radiation in spatially separated targets is studied in the presence of ultrasound (US) vibrations in one of the targets. The time evolution of the nuclear exciton perturbed in such a way is described by interference between the wave packets re-emitted by both targets and radiative coupling between the targets. Since the condition for initial phasing of the wave packets and coupling can be restored periodically by US, strong intensity enlargements in the time response, called nuclear exciton echoes, are observed. If the targets have different resonant energies quantum beats arise which are frequency modulated by the US perturbation. A complete dynamical theory is presented which provides a quantitative description of all experimental results discussed.

1. Introduction

In nuclear resonant scattering of Mössbauer or synchrotron radiation (SR) an excited nuclear state delocalized over an ensemble of nuclei is created. In such a state, which is often called a nuclear exciton, each nucleus of the ensemble is excited by the incident γ quantum with a certain probability amplitude. The excitation by a SR pulse occurs almost instantaneously compared with the nuclear lifetime. So after the short SR pulse the exciton develops with time and exhibits a free coherent decay, which, however, can be perturbed by an inherent stochastic motion of the nuclei themselves or by that of their environment (diffusion, relaxation) or by dynamics caused externally in a specific and controllable way (rf magnetic or ultrasound excitation of a target).

When describing the evolution of a nuclear exciton in space and time one has to consider a united system where the two sub-systems, the γ-ray field and the nuclear transition currents, are dynamically coupled to each other. The state of the united system is developing in space occupied by the nuclear ensemble. As pointed out earlier [1], there exist scattering geometries, in particular the forward scattering geometry, where one nuclear exciton can extend over several spatially separated targets. This occurs because the SR pulse creates phased nuclear excitation of all targets in space and time. The spatial phasing allows the exciton which comprises all targets involved to decay coherently via radiative emission into the forward direction.

As an example, in this contribution we describe experiments where the nuclear exciton extends over two stainless steel targets A and B that are spatially separated but otherwise identical. The nuclear exciton created in the combined target is perturbed in a controllable way by subjecting one of the two targets to ultrasound (US).

The response of the total target can be presented by the sum of the responses of the targets A and B and of the term describing radiative coupling of these targets (see [1, section 6]). The effect of the US perturbation on the total response originates from two sources: (a) the periodic change of the interference between the A and B responses caused by the modulation of the relative phase between them, and (b) the periodic destruction and restoration of the radiative coupling of the targets because of the relative motion of their resonances. The latter effect is dominant if $ka\Omega \leqslant \Gamma$, where k is the radiation wave number, a and Ω are the US vibration amplitude and frequency, respectively, and Γ is the natural width of the nuclear level, while the first effect dominates if $ka\Omega \gg \Gamma$. The relevance of both, interference and coupling, will be discussed in section 2.

The role of radiative coupling can also be controlled by a variation of the energy separation of the resonances in the targets. This can be accomplished, for example, by moving one target with constant velocity v relative to the second target. In this respect, two types of experiments will be described, one allowing for the radiative coupling between the targets and the other excluding it for almost the whole time.

In the first type, the nuclei of targets A and B have the same resonance energy $\hbar\omega_0$. Therefore, the nuclei of A and B are strongly coupled via the γ radiation field in the absence of relative motion of the targets. The nuclear exciton extending over A and B is perturbed by moving one target by sinusoidal ultrasound. Since the vibration is periodic, the initial phasing of the A and B responses and the coupling can periodically be restored leading to a strong increase of intensity in the time dependence. These intensity peaks are called *nuclear exciton echoes*.

In the second type of experiments the nuclei in A and B have different resonant energies. This is achieved by moving one target with constant velocity v relative to the stationary target. Due to the difference $\hbar\Delta\omega$ in resonant energies a quantum beat (QB) arises with a period of $2\pi/\Delta\omega$. In this case, if $v \gg \Gamma$ there is almost no coupling between the nuclei in A and B at all times. In addition to the constant velocity v, a perturbation is introduced by moving the stationary target by sinusoidal ultrasound. This causes a frequency modulation of the QB. Echo-like phenomena can also arise in such experiments.

In section 2 the formulae are derived for the forward scattering intensity from the two-part target with one part being moved by a US driver. The formulae were used for fitting the experimental time spectra in various cases. Section 3 presents experimental details. In section 4, experimental results are described and discussed. A summary is given in section 5.

2. Theory

2.1. Propagation of SR pulses through an US vibrated single-line resonant target

An elementary theoretical approach in terms of the classical optical theory is developed. In order to make the physical processes more transparent we first neglect electronic absorption. This, as well as inhomogeneous line broadening will be taken into account later (see eq. (2.20)).

2.1.1. Solution in the energy domain

We assume the nuclear media to be optically isotropic and to exhibit a nuclear resonance of Lorentzian shape. Let the nuclear absorber be a plane parallel platelet set perpendicular to the z-axis with the entrance surface at $z = 0$. The z-axis is the propagation axis of the SR pulse. Let the absorber as a whole be put in the oscillatory motion along the z-axis by a US driver at frequency Ω. The deviation of the absorber at time t from the equilibrium position is given by

$$u(t) = a \sin(\Omega t + \Phi), \tag{2.1}$$

where a and Φ are the oscillation amplitude and initial phase, respectively. A broad energy band of SR containing the resonance energy is selected by a monochromator system. We assume all energy components to be of equal amplitude

$$\varepsilon_{\omega_0} = \sqrt{\frac{I_0}{\Delta\omega}} \tag{2.2}$$

in a wide resonance range $\Delta\omega$ selected by the monochromator, where I_0 is the intensity of the selected SR and ω_0 is the nuclear resonance frequency.

Let us consider the propagation of a Fourier component of SR, $E_\omega = \varepsilon_{\omega_0}\, \mathrm{e}^{\mathrm{i}(\omega t - kz)}$, through the nuclear absorber, with k the wave vector. Initially we solve the propagation problem in the system where the absorber is at rest. In this system the Fourier component is phase modulated, so that

$$E'_\omega = \varepsilon_{\omega_0}\, \mathrm{e}^{\mathrm{i}\{\omega t - k[z+u(t)]\}} = \varepsilon_{\omega_0}\, \mathrm{e}^{\mathrm{i}(\omega t - kz) - \mathrm{i}ka\sin(\Omega t + \Phi)}. \tag{2.3}$$

Applying the Jakoby–Anger relationship $\mathrm{e}^{-\mathrm{i}w\sin\varphi} = \sum_{-\infty}^{+\infty} J_n(w)\, \mathrm{e}^{-\mathrm{i}n\varphi}$, where $J_n(w)$ is the Bessel function of real argument and nth order, and the argument $w = ka$ is the modulation index, we can present the modulated wave as a set of "harmonics"

$$E'_{\mathrm{inc}} = \varepsilon_{\omega_0}\, \mathrm{e}^{\mathrm{i}(\omega t - kz)} \sum_{n=-\infty}^{+\infty} J_n(w)\, \mathrm{e}^{-\mathrm{i}n(\Omega t + \Phi)} \tag{2.4}$$

with amplitudes $\varepsilon_{\omega_0} J_n(w)$, frequencies $\omega + n\Omega$, and phases shifted by steps of $n\Phi$.

One can readily find the solution for each harmonic transmitted through the target (see [1, section 5.1]):

$$E'_{\mathrm{tr}}(\omega - n\Omega) = \varepsilon_{\omega_0} \cdot J_n(w) \cdot \mathrm{e}^{\mathrm{i}[(\omega - n\Omega)t - n\Phi] - \mathrm{i}(\omega/c)(1+\eta_{\mathrm{n}}/2)z}, \tag{2.5}$$

where $\eta_{\rm n}$ is the nuclear susceptibility defined for the given conditions as

$$\eta_{\rm n} = -\frac{c}{\omega}\mu_{\rm r}\frac{\Gamma/2\hbar}{\omega-\omega_0-n\Omega-{\rm i}\Gamma/2\hbar}, \tag{2.6}$$

where $\mu_{\rm r}$ is the linear nuclear absorption coefficient at resonance, Γ is the natural width of the nuclear levels in the excited state.

The total transmitted field is the coherent superposition of the contributions given by eq. (2.5):

$$E'_{\rm tr}(\omega) = \varepsilon_{\omega_0}\sum_{n=-\infty}^{+\infty} J_n(w)\cdot {\rm e}^{{\rm i}[(\omega-n\Omega)t-n\Phi]}\cdot {\rm e}^{{\rm i}\frac{T/2}{2(\omega-\omega_0-n\Omega)t_0-{\rm i}}}, \tag{2.7}$$

where $T=\mu_{\rm r}z$ is a dimensionless thickness parameter often called the effective thickness of the nuclear resonance absorber (Mössbauer thickness), $t_0=\hbar/\Gamma$ is the natural lifetime, and the phase factor ${\rm e}^{-{\rm i}(\omega/c)z}$, taking into account the optical path of a wave in vacuum, is omitted in eq. (2.7). For going back to the laboratory system one has to multiply eq. (2.7) by $\exp[{\rm i}w\sin(\Omega t+\Phi)]$, so that

$$E_{\rm tr}(\omega) = \varepsilon_{\omega_0}\,{\rm e}^{{\rm i}w\sin(\Omega t+\Phi)}\sum_{n=-\infty}^{+\infty} J_n(w)\cdot {\rm e}^{{\rm i}[(\omega-n\Omega)t-n\Phi]}\cdot {\rm e}^{{\rm i}\frac{T/2}{2(\omega-\omega_0-n\Omega)t_0-{\rm i}}}. \tag{2.8}$$

Thus each Fourier component of SR is transformed into a set of harmonics with frequencies $\omega+n\Omega$, and each harmonic turns out to be phase modulated at an US frequency due to the interaction with the vibrated absorber.

2.1.2. Solution in the time domain

Now we integrate all oscillations given by eq. (2.8) to get the wave packet of radiation transmitted through the vibrated target:

$$E_{\rm tr}(t) = \frac{1}{2\pi}\int_{-\infty}^{+\infty}{\rm d}\omega E_{\rm tr}(\omega),$$

the infinite limits are taken in the assumption that SR has a δ-function time structure. As a result there is a sum of integrals at different n. Omitting the pre-integral factor we have the following partial integral to be evaluated:

$$S_l = \frac{1}{2\pi}\int_{-\infty}^{+\infty}{\rm d}\omega\cdot {\rm e}^{{\rm i}\omega t}{\rm e}^{{\rm i}\frac{T/2}{2(\omega-\omega_0-l\Omega)t_0-{\rm i}}}. \tag{2.9}$$

A similar integral was considered in [2] and we apply the result given there for our case

$$S_l = \delta(t) - \frac{T}{2t_0}\cdot {\rm e}^{{\rm i}(\omega_0+l\Omega)t-\tau/2}\cdot\sigma(T\tau) \tag{2.10}$$

with $\sigma(T\tau) = J_1(\sqrt{T\tau})/\sqrt{T\tau}$, where J_1 is the Bessel function of real argument and first order and $\tau = t/t_0$ is the reduced time, $\delta(t)$ is the Dirac δ-function. Making use of eq. (2.10) we write the solution for the transmitted wave packet:

$$E_{\rm tr}(t) = \varepsilon_{\omega_0} \mathrm{e}^{\mathrm{i}w\,\sin(\Omega t+\Phi)} \sum_{n=-\infty}^{+\infty} J_n(w) \cdot \mathrm{e}^{-\mathrm{i}n(\Omega t+\Phi)} \times \left[\delta(t) - \frac{T}{2t_0} \cdot \mathrm{e}^{\mathrm{i}(\omega_0+n\Omega)t-\tau/2} \cdot \sigma(T\tau)\right]. \tag{2.11}$$

Applying again the Jakoby–Anger formula we obtain the final solution for the wave packet transmitted through the vibrating target

$$E_{\rm tr}(t) = \varepsilon_{\omega_0} \left\{ \delta(t) - \frac{T}{2t_0} \cdot \mathrm{e}^{\mathrm{i}\omega_0 t+\mathrm{i}w[\sin(\Omega t+\Phi)-\sin\Phi]-\tau/2} \cdot \sigma(T\tau) \right\}. \tag{2.12}$$

Time $t = 0$ marks the arrival of the SR pulse at the detector. The solution given by eq. (2.12) is different from the solution for the target at rest by the additional time-dependent phase $w[\sin(\Omega t + \Phi) - \sin\Phi]$ in the exponential. Since the detector is not sensitive to the radiation phase this additional phase factor does not change the time dependence of the scattered intensity. So the scattering intensity cannot reveal the target vibration [3,4]. A theory describing the time evolution of Bragg and forward scattering of SR from a nuclear ensemble subjected to US vibrations is presented in [5].

2.2. Propagation of SR pulses through two targets one of which is US vibrated

2.2.1. Solution in the energy domain

The scattering arrangement shown in figure 1 is considered. The large bandwidth of the SR is in a first step reduced by a standard Si (1 1 1) monochromator, and further monochromatized to a bandwidth of several meV by a 4-bounce nested monochromator. After passing through targets A and B the γ radiation is detected by a fast avalanche photodiode (APD). Let each constituent target again have a single-line resonance. To reduce the task to the former case we assume that the up-stream A-target is at rest while the down-stream B-target is US moved (later it will be proved that the two targets are commutative, see also [1]).

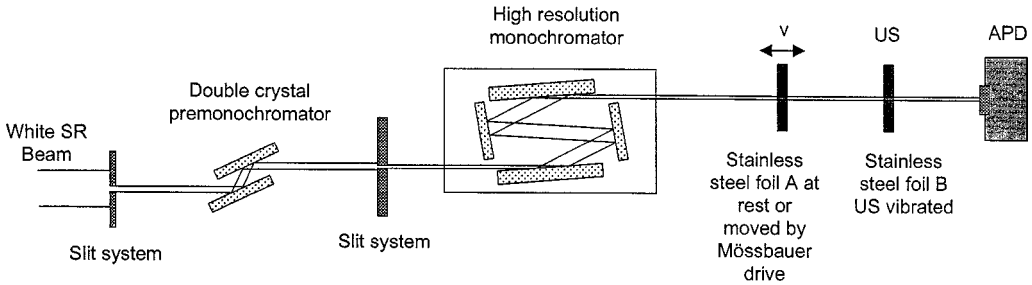

Figure 1. Experimental setup involving two separated targets A and B.

A Fourier component of incident radiation $\varepsilon_{\omega_0}\,\mathrm{e}^{\mathrm{i}\omega t}$ is transformed into

$$\varepsilon''_{\omega} = \varepsilon_{\omega_0}\,\mathrm{e}^{\mathrm{i}\omega t}\,\mathrm{e}^{\mathrm{i}\frac{T_\mathrm{A}/2}{2(\omega-\omega_\mathrm{A})t_0-\mathrm{i}}} \tag{2.13}$$

due to transmission through the A-target. In eq. (2.13), T_A and ω_A are the effective resonant thickness and resonant frequency of the up-stream target. The monochromatic wave with reduced amplitude and shifted in phase given by eq. (2.13) is now incident on the vibrating target and is further transformed in accordance with eq. (2.8):

$$\begin{aligned} E_\mathrm{tr}(\omega) = \varepsilon_{\omega_0}\,&\mathrm{e}^{\mathrm{i}\frac{T_\mathrm{A}/2}{2(\omega-\omega_\mathrm{A})t_0-\mathrm{i}}}\,\mathrm{e}^{\mathrm{i}w\sin(\Omega t+\Phi)} \\ &\times \sum_{n=-\infty}^{+\infty} J_n(w)\cdot\mathrm{e}^{\mathrm{i}[(\omega-n\Omega)t-n\Phi]}\cdot\mathrm{e}^{\mathrm{i}\frac{T_\mathrm{B}/2}{2(\omega-\omega_\mathrm{B}-n\Omega)t_0-\mathrm{i}}}, \end{aligned} \tag{2.14}$$

where T_B and ω_B are the effective resonant thickness and resonant frequency of the vibrating target. Thus eq. (2.15) represents a wave emerging from the two targets where one target (B) is US vibrated. It is a partial wave of the total field of the SR flash.

2.2.2. Solution in the time domain I

We obtain the transmitted wave packet by integrating over all oscillations given by eq. (2.15). Let us find the solution for the nth integral (the pre-integral factor will again be omitted, except for the Bessel function):

$$S_n = \frac{J_n}{2\pi}\int_{n=-\infty}^{+\infty}\mathrm{d}\omega\cdot\mathrm{e}^{\mathrm{i}\omega t}\,\mathrm{e}^{\mathrm{i}\frac{T_\mathrm{A}/2}{2(\omega-\omega_\mathrm{A})t_0-\mathrm{i}}}\,\mathrm{e}^{\mathrm{i}\frac{T_\mathrm{B}/2}{2(\omega-\omega_\mathrm{B}-n\Omega)t_0-\mathrm{i}}}. \tag{2.15}$$

First we consider the particular case where $\omega_\mathrm{A}=\omega_\mathrm{B}=\omega_0$.

The integral for $n=0$ is similar to that given by eq. (2.9). So we can immediately write down the solution:

$$S_0 = J_0\left[\delta(t) - \frac{T_\mathrm{AB}}{2t_0}\cdot\mathrm{e}^{\mathrm{i}\omega_0 t-\tau/2}\cdot\sigma(T_\mathrm{AB}\tau)\right], \tag{2.16}$$

where $T_\mathrm{AB}=T_\mathrm{A}+T_\mathrm{B}$ and

$$\sigma(T_\mathrm{AB}\tau) = \frac{J_1(\sqrt{(T_\mathrm{A}+T_\mathrm{B})\tau})}{\sqrt{(T_\mathrm{A}+T_\mathrm{B})\tau}}.$$

The evaluation of an integral with $n\neq 0$ is given in the appendix. This solution is as follows:

$$S_n = J_n\left\{\delta(t) - \frac{1}{2t_0}\,\mathrm{e}^{\mathrm{i}\omega_0 t-\tau/2}\left[\mathrm{e}^{-\mathrm{i}\frac{T_\mathrm{B}}{4n\Omega t_0}}(T\sigma)_\mathrm{A} + \mathrm{e}^{\mathrm{i}n\Omega t}\,\mathrm{e}^{\mathrm{i}\frac{T_\mathrm{A}}{4n\Omega t_0}}(T\sigma)_\mathrm{B}\right]\right\}, \tag{2.17}$$

where $(T\sigma)_{\rm A} = T_{\rm A}\cdot\sigma(T_{\rm A}\tau)$ and analogous for $(T\sigma)_{\rm B}$. We finally arrive at the following solution for the transmitted wave packet:

$$E_{\rm tr}(t) = \varepsilon_{\omega_0}\delta(t) - \varepsilon_{\omega_0}\frac{1}{2t_0}\,{\rm e}^{{\rm i}\omega_0 t + {\rm i}w\sin(\Omega t+\Phi)-\tau/2} \times\left[J_0(T\sigma)_{\rm AB} + \sum_{n\neq 0} J_n\,{\rm e}^{-{\rm i}n\Phi}\left({\rm e}^{-{\rm i}n\Omega t}\,{\rm e}^{-{\rm i}\frac{T_{\rm B}}{4n\Omega t_0}}(T\sigma)_{\rm A} + {\rm e}^{{\rm i}\frac{T_{\rm A}}{4n\Omega t_0}}(T\sigma)_{\rm B}\right)\right], \quad (2.18)$$

where $(T\sigma)_{\rm AB} = (T_{\rm A}+T_{\rm B})\sigma(T_{\rm AB}\tau)$.

Let us write down separately the delayed part, i.e., the nuclear forward scattered part of this packet:

$$E_{\rm fs}(t) = -\varepsilon_{\omega_0}\frac{1}{2t_0}\,{\rm e}^{{\rm i}\omega_0 t + {\rm i}w\sin(\Omega t+\Phi)-\tau/2}\left[J_0(T\sigma)_{\rm AB} + \sum_{n\neq 0} J_n\,{\rm e}^{-{\rm i}n\Phi} \times\left({\rm e}^{-{\rm i}n\Omega t}\,{\rm e}^{-{\rm i}\frac{T_{\rm B}}{4n\Omega t_0}}(T\sigma)_{\rm A} + {\rm e}^{{\rm i}\frac{T_{\rm A}}{4n\Omega t_0}}(T\sigma)_{\rm B}\right)\right]. \quad (2.19)$$

Using eq. (2.19) we calculate the forward scattered intensity in the absence of synchronization between SR pulse and US phase. In this case one should average the forward scattered intensity over the US phase Φ: $I_{\rm fs} = \langle E_{\rm fs}\cdot E_{\rm fs}^{*}\rangle_{\Phi}$. The product of the sum in eq. (2.19) and its complex conjugate value contains terms with different n. Due to averaging over Φ these cross terms vanish and we obtain the following formula for the time dependence of the scattered intensity:

$$I_{\rm fs}(t,w) = I_0\frac{\Gamma}{\Delta E}\,\frac{1}{4t_0}\,{\rm e}^{-T_e}\,{\rm e}^{-q\tau}\left\{J_0^2(w)\cdot(T\sigma)_{\rm AB}^2 + 2\sum_{n=1}^{\infty}J_n^2(w) \times\left[(T\sigma)_{\rm A}^2 + (T\sigma)_{\rm B}^2 + 2(T\sigma)_{\rm A}(T\sigma)_{\rm B}\cos\left(n\Omega t + \frac{T_{\rm AB}}{4n\Omega t_0}\right)\right]\right\}. \quad (2.20)$$

We included in the expression for the intensity the factor ${\rm e}^{-T_e}$ accounting for the electronic absorption, T_e being the electronic effective thickness. We have replaced ${\rm e}^{-\tau}$ by ${\rm e}^{-q\tau}$ where q accounts for the resonance broadening (see, e.g., [6, section 2.4.3]).

We now consider the case where $\omega_{\rm A}\neq\omega_{\rm B}$. Again we choose a particular case corresponding to experimental conditions, namely, where $(\omega_{\rm B}-\omega_{\rm A})t_0 = \Delta\omega t_0 \gg 1$, and $\Delta\omega \gg n_u\Omega$, where n_u denotes the term at which the sum containing the Bessel functions can be truncated. Under these conditions all integrals in eq. (2.15) are similar to that evaluated in the appendix. The result of integration is the same as that given by eq. (2.17), with $n\Omega$ replaced by $\Delta\omega + n\Omega$. After these comments we can immediately write down the answer for the forward scattering intensity:

$$I_{\rm fs}(t,w) = I_0 \frac{\Gamma}{\Delta E}\,\frac{1}{4t_0}\,{\rm e}^{-T_e}\,{\rm e}^{-q\tau}\sum_{n=-\infty}^{+\infty} J_n^2(w)\Big\{(T\sigma)_{\rm A}^2 + (T\sigma)_{\rm B}^2 + 2(T\sigma)_{\rm A}(T\sigma)_{\rm B}\cos\Big[(\Delta\omega + n\Omega)t + \frac{T_{\rm AB}}{4(\Delta\omega + n\Omega)t_0}\Big]\Big\}. \quad (2.21)$$

2.2.3. Solution in the time domain II

In this subsection we find the expression for the wave packet transmitted through the two targets using the time response function technique as done in [1, section 6.1, eq. (54)]. As the time response of the US vibrated target we use the expression in the curly brackets in eq. (2.12):

$$E_{\rm tr}(t) = \varepsilon_{\omega_0}\int_0^t {\rm d}t'\cdot\Big[\delta\big(t'\big) - \frac{T_{\rm A}}{2t_0}\cdot{\rm e}^{{\rm i}\omega_0 t' - \tau'/2}\cdot\sigma\big(T_{\rm A}\tau'\big)\Big] \times\Big\{\delta\big(t-t'\big) - \frac{T_{\rm B}}{2t_0}\cdot{\rm e}^{{\rm i}(\omega_0+\Delta\omega)(t-t')+{\rm i}w\{\sin[\Omega(t-t')+\Phi]-\sin\Phi\}-(\tau-\tau')/2} \times\sigma\big[T_{\rm B}\big(\tau-\tau'\big)\big]\Big\}, \quad (2.22)$$

where t' and t are the excitation and de-excitation time of nuclei in the down-stream target, respectively. Time zero marks the arrival of the SR pulse at the detector. The shift $\Delta\omega$ of resonances in the targets is taken into account. The expression in the square brackets of the upper line of eq. (2.22) represents the time dependence of the exciting field, that is the δ-pulse and the $E_{\rm A}$-field emerging from the first target, while the expression in the curly brackets of the lower lines of eq. (2.22) represents the response of the down-stream US vibrated target. While executing the integration we use the relationship $\int {\rm d}x\cdot\delta(x)\cdot f(a-x) = f(a)$, and arrive at

$$E_{\rm tr}(t) = \varepsilon_{\omega_0}\Big\{\delta(t) - \frac{1}{2t_0}\,{\rm e}^{{\rm i}\omega_0 t-\tau/2}\Big[(T\sigma)_{\rm A} + {\rm e}^{{\rm i}\Delta\omega t+{\rm i}w\{\sin[\Omega t+\Phi]-\sin\Phi\}}(T\sigma)_{\rm B} - \frac{T_{\rm A}T_{\rm B}}{2t_0}\int_0^t {\rm d}t'\cdot{\rm e}^{{\rm i}\Delta\omega(t-t')+{\rm i}w\{\sin[\Omega(t-t')+\Phi]-\sin\Phi\}}\cdot\sigma\big(T_{\rm A}\tau'\big) \times\sigma\big[T_{\rm B}\big(\tau-\tau'\big)\big]\Big]\Big\} \quad (2.23)$$

with $\tau' = t'/t_0$.

The expression in the curly brackets is the time response function of the two targets where one target is US vibrated. It allows one to find the forward scattering intensity when an arbitrary US phase is locked to the SR pulse and when an arbitrary shift of the resonances is present. From the structure of the expression it is immediately seen that it is invariant to the sequence of the targets. Indeed the inversion of the target sequence results in mutual replacement of the time variables $t' \Longleftrightarrow t - t'$ in eq. (2.22). The same exchange of variables takes place in the integrand of eq. (2.23). Taking into account that $-\int_t^0 {\rm d}t' = \int_0^t {\rm d}t'$ we immediately see that the system is reversible.

The last term in eq. (2.23) describes the radiative coupling between the targets, as discussed in [1]. However, when the separation between the resonances in the targets is large, $\Delta\omega t \gg w$ in the observation window, the role of radiative coupling is vanishing and we obtain for the transmitted wave packet

$$E_{\rm tr}(t) = \varepsilon_{\omega_0}\left\{\delta(t) - \frac{1}{2t_0}\,\mathrm{e}^{\mathrm{i}\omega_0 t-\tau/2}\left[(T\sigma)_{\rm A} + \mathrm{e}^{\mathrm{i}\Delta\omega t+\mathrm{i}w\{\sin[\Omega t+\Phi]-\sin\Phi\}}(T\sigma)_{\rm B}\right]\right\} \quad (2.24)$$

or for its delayed part

$$E_{\rm fs}(t) = -\varepsilon_{\omega_0}\frac{1}{2t_0}\,\mathrm{e}^{\mathrm{i}\omega_0 t-\tau/2}\left[(T\sigma)_{\rm A} + \mathrm{e}^{\mathrm{i}\Delta\omega t+\mathrm{i}w\{\sin[\Omega t+\Phi]-\sin\Phi\}}(T\sigma)_{\rm B}\right]. \quad (2.25)$$

2.2.4. Conclusions of the theory

Here we put together the formulae obtained above for the forward scattered intensity from the two targets which were used for fitting the experimental time spectra in the various cases.

1. SR pulse and US motion are not synchronized and there is no energy separation between the resonances in the up/down-stream targets (eq. (2.20)):

$$I_{\rm fs}(t,w) = I_0\frac{\Gamma}{\Delta E}\,\frac{1}{4t_0}\,\mathrm{e}^{-T_e}\,\mathrm{e}^{-q\tau}\left\{J_0^2(w)\cdot(T\sigma)_{\rm AB}^2 + 2\sum_{n=1}^{\infty}J_n^2(w) \times\left[(T\sigma)_{\rm A}^2 + (T\sigma)_{\rm B}^2 + 2(T\sigma)_{\rm A}(T\sigma)_{\rm B}\cos\left(n\Omega t + \frac{T_{\rm AB}}{4n\Omega t_0}\right)\right]\right\}. \quad (2.26)$$

2. SR pulse and US motion are not synchronized and the separation between the resonances in the up/down-stream targets is large (eq. (2.21)):

$$I_{\rm fs}(t,w) = I_0\frac{\Gamma}{\Delta E}\,\frac{1}{4t_0}\,\mathrm{e}^{-T_e}\,\mathrm{e}^{-q\tau}\sum_{n=-\infty}^{+\infty}J_n^2(w)\left\{(T\sigma)_{\rm A}^2 + (T\sigma)_{\rm B}^2 + 2(T\sigma)_{\rm A}(T\sigma)_{\rm B}\cos\left[(\Delta\omega + n\Omega)t + \frac{T_{\rm AB}}{4(\Delta\omega+n\Omega)t_0}\right]\right\}. \quad (2.27)$$

We note that both the expression in eq. (2.26) and that in eq. (2.27) are invariant to an inversion of the target parts. Thus the commutativity of the system also holds in the case of US phase averaging.

3. When the SR pulse is locked to the US-motion phase and the energy separation between the resonances in the two targets is large, we have the following expression for the forward scattering intensity:

$$I_{\rm fs}(t,w) = I_0\frac{\Gamma}{\Delta E}\,\frac{1}{4t_0}\,\mathrm{e}^{-T_e}\,\mathrm{e}^{-q\tau}\left\{(T\sigma)_{\rm A}^2 + (T\sigma)_{\rm B}^2 + 2(T\sigma)_{\rm A}(T\sigma)_{\rm B}\cos\left\{\Delta\omega t + w\left[\sin(\Omega t+\Phi) - \sin\Phi\right]\right\}\right\}, \quad (2.28)$$

which is readily obtained using eq. (2.25). As mentioned above, q accounts for the resonance broadening.

4. The time dependence of the intensity in the case of synchronized US motion and an arbitrary resonance shift has to be found numerically using eq. (2.23), omitting its prompt part.

The formulae given above are valid for a coherent piston-like motion of the nuclear target. In the case of inhomogeneous motion one should average the scattering intensity over the relevant distribution of the US amplitude in the target area.

5. How important is the last term in eq. (2.23) which describes the radiative coupling between the targets, as compared to the other terms responsible for the interference between the A and B wave packets? Obviously this depends on $\Delta\omega$ and on w. If $\Delta\omega \leqslant \Gamma$ and $w\Omega \leqslant \Gamma$ the coupling term is comparable in magnitude to the interference term and is important in the whole time window of the experiment (typically, 250 ns). The sum of both terms determines the overall shape of the nuclear decay time dependence. If $\Delta\omega > \Gamma$, the importance of the coupling term is reduced because of the energy separation of the resonances. In the energy domain, if $w\Omega > \Gamma$, the coupling is reduced because of the creation of sidebands at $\omega_0 \pm n\Omega$. In this case the coupling term becomes less important because the radiation frequency is shifted from the carrier into the sidebands. The forward scattering is then determined mainly by the interference term.

6. Concerning the echo effects, the basic ideas can be derived from kinematical theory, where the interaction of the re-emitted wave field from target A with the nuclei in target B is neglected. However, one should keep in mind that the kinematical theory is an approximation. As pointed out in the previous comment (5), for a quantitative description of experiments the equations derived above within the dynamical theory ought to be used.

At time $t = 0$ of the excitation by the SR pulse an exciton is formed which extends over both targets. As a consequence, at $t = 0$ the emission in the forward direction is characteristic for the combined target of thickness ($T_\mathrm{A}+T_\mathrm{B}$), regardless of the amplitude and phase of the US vibration. At later times, however, this exciton starts to be disrupted by the US vibration. Separate excitons form and develop differently in time.

Let us first consider case 1, where both targets have the same resonance, i.e., $\Delta\omega = 0$; the SR pulse is locked to the phase of the US motion. Neglecting radiative coupling between targets we omit the last term in eq. (2.23) and analogous to eq. (2.28) we find for the delayed radiation intensity

$$I_\mathrm{fs}(t,w) = I_0 \frac{\Gamma}{\Delta E}\,\frac{1}{4t_0}\,\mathrm{e}^{-T_e}\,\mathrm{e}^{-q\tau}\big\{(T\sigma)_\mathrm{A}^2 + (T\sigma)_\mathrm{B}^2 + 2(T\sigma)_\mathrm{A}(T\sigma)_\mathrm{B}\cos\big\{w\big[\sin(\Omega t+\Phi)-\sin\Phi\big]\big\}\big\}. \tag{2.29}$$

The phase difference between the responses of the targets A and B is given by

$$\Psi(t) = w\big[\sin(\Omega t+\Phi)-\sin\Phi\big] = (2\pi/\lambda)\big[u(t)-u(0)\big] \tag{2.30}$$

where we have used eq. (2.1).

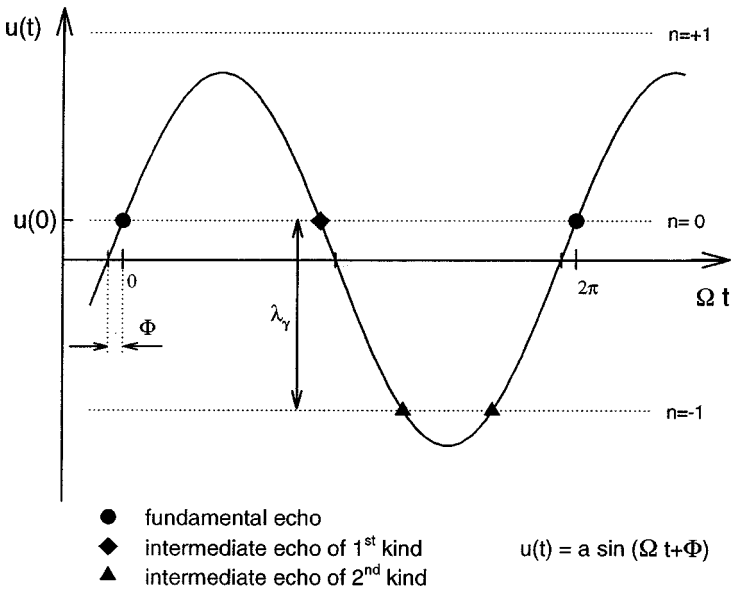

Figure 2. Sinusoidal displacement $u(t)$ of the resonant nuclei in the US vibrated target. Echoes can be observed when $u(t) - u(0) = n\lambda$. Three types of nuclear exciton echoes can be distinguished: fundamental echoes after full periods of the US motion ($n = 0$); intermediate echoes of 1st kind ($n = 0$) and intermediate echoes of 2nd kind ($n = \pm 1, \pm 2, \ldots$).

Rephasing occurs when the displacement $u(t)$ differs from its initial value $u(0)$ at $t = 0$ by multiples of the radiation wavelength λ: $[u(t) - u(0)] = n\lambda$, whereas intensity minima are observed at $[u(t) - u(0)] = (2n + 1)\lambda/2$, where $n = 0, \pm 1, \pm 2, \ldots$.

When rephasing occurs, constructive interference leads to maxima in the forward emission intensity (for equally thick targets; the case of unequally thick targets is considered in section 4.1 below). These maxima are called nuclear exciton echoes.

Figure 2 shows that three types of echo can be distinguished:

(1) fundamental echoes, where rephasing happens after each US period P, when $n = 0$,

(2) intermediate echoes of the 1st kind, where $u(0)$ is reached between fundamental echoes, again with $n = 0$,

(3) intermediate echoes of the 2nd kind, where $u(0) + n\lambda$, with $n = \pm 1, \pm 2, \ldots$ is reached.

We consider now case 2 where the energy separation $\Delta\omega$ between resonances of the two targets is large. According to eq. (2.28), the relative phase $\Psi(t)$ between the radiation fields from targets A and B is given by

$$\Psi(t) = \Delta\omega t + w\big[\sin(\Omega t + \Phi) - \sin\Phi\big] = \Delta\omega t + (2\pi/\lambda)\big[u(t) - u(0)\big], \qquad (2.31)$$

with $\Delta\omega t \gg w$.

The energy separation $\Delta\omega$ gives rise to a quantum beat (QB) with local intensity maxima at times $t = l(2\pi/\Delta\omega)$ and local minima at $t = (2l + 1)(\pi/\Delta\omega)$, where $l = 0, 1, 2, \ldots$. However, overall maxima are observed at those times (in good approximation, since $\Delta\omega t \gg w$) where in addition $[u(t) - u(0)] = n\lambda$, and overall minima at $[u(t) - u(0)] = (2n + 1)\lambda/2$. An additional interesting aspect is the frequency modulation of the QB. The instantaneous frequency ω_i is given by

$$\Delta\omega_i = \frac{\mathrm{d}\Psi(t)}{\mathrm{d}t} = \frac{\mathrm{d}}{\mathrm{d}t}\left\{\Delta\omega t + w\left[\sin(\Omega t + \Phi) - \sin\Phi\right]\right\} \tag{2.32}$$

or $\Delta\omega_i = \Delta\omega + w\Omega\cos(\Omega t + \Phi)$, i.e., the frequency of the QB varies between $\Delta\omega - w\Omega$ and $\Delta\omega + w\Omega$, depending on the modulation index (amplitude) w of the US motion.

3. Experimental details

Experiments were performed at the storage rings of the Stanford Synchrotron Radiation Laboratory (SSRL), the Hamburg Synchrotron Laboratory (HASYLAB), the European Synchrotron Radiation Facility (ESRF), and of the National Laboratory for High Energy Physics (KEK), Japan. The experimental setup is depicted in figure 1. The radiation energy of 14.413 keV for the ^{57}Fe resonance is first defined by a standard Si (1 1 1) monochromator, and then further monochromatized to a bandwidth of several meV by a 4-bounce nested high-resolution monochromator. After passing through targets A and B the γ radiation is detected by a fast avalanche photodiode (APD).

3.1. Piezoelectric vibrations

For most of the US experiments stainless steel (SS) foils ($Fe_{55}Cr_{25}Ni_{20}$, enriched to 95% in ^{57}Fe) of $\sim$ 1 μm thickness were used as targets A and B. Target A was either kept at rest or moved at constant velocity by a conventional electromechanical Mössbauer drive. The SS foil of target B was cut to a diameter of 5 mm and then glued to a piezodriver which produced the US motion. This piezodriver with target B was mounted at a distance of typically 20 cm downstream from foil A.

Two types of piezodriver were employed: quartz single crystals and piezofoils made from polyvinylidene fluoride (PVDF) [7]. The X-cut quartz crystals were of 20 mm diameter and 0.19 mm thickness. They were vibrated near their thickness resonance of $\sim$14.5 MHz. The vibration amplitude was adjusted by applying rf-voltages between 0 and 10 Volts. Although the diameter of the SS foil is much smaller than that of the quartz crystal the US motion is not homogeneous over the area of the SS foil, i.e., it is only partially piston-like. The motion of the major part of the SS foil is characterized by a Rayleigh distribution of vibration amplitudes. In applications where piston-like motion is required, this problem can be remedied to a large extent by employing PVDF foils. In this case drivers of 110 μm thickness were used [8]. When operated at rf frequencies up to 12 MHz with rf voltages up to $\sim$20 V such PVDF foils exhibit mainly piston-like motion. For both types of drivers vibration amplitudes a

up to 1.5 times the γ-ray wavelength ($\lambda = 0.86$ Å) can be easily achieved. This corresponds to a modulation index $w = 2\pi a/\lambda \approx 10$.

3.2. Magnetoelastic vibrations

The magnetoelastic effect was used to produce coherent vibrations of resonant nuclei in a $^{57}FeBO_3$ single crystal enriched to 95% in ^{57}Fe. The sample was a platelet of 4.2×6.2 mm^2 and the crystal surface coincided with the (1 1 1) plane [9,10]. In order to selectively excite the nuclear transitions $\Delta m = 0$ in ^{57}Fe a static magnetic field of 10 Oe was applied parallel to the crystal surface, bringing the crystal into the single domain state where hyperfine magnetic fields were aligned along the magnetic polarization vector of the X-rays. A radio-frequency (rf) magnetic field was applied parallel to the crystal surface and perpendicular to the static field with a peak amplitude of 15 Oe at a frequency of 2.384 MHz. The composite of the static and rf magnetic fields, which determines the direction of the crystal magnetization, oscillates between $+56^\circ$ and -56° around the static magnetic field. Due to the magnetoelastic effect the ^{57}Fe nuclei vibrate coherently along the X-ray beam path in the crystal. The vibration amplitudes of the ^{57}Fe nuclei depend on the depth in the crystal and vary between 0 and a maximal value at the front and back crystal surfaces, respectively. For further details see [9,10].

3.3. Synchronization of the vibrations with the SR pulse

In some experiments it is desirable to synchronize the excitation of the targets by the SR pulses with the US motion of the resonant nuclei. This can easily be achieved by a phase-locked-loop circuit which locks the output of an rf generator to a timing signal from the storage ring. This timing signal first passes an adjustable delay box and then drives the synchronization stage of the rf generator. The delay box allows variation of the phase difference between the SR emission and the US motion.

4. Results and discussion

4.1. Targets coupled via the radiation field

In the first type of experiments the resonant energies of the nuclei in targets A and B are the same. Therefore the nuclei of both targets are strongly coupled via the γ radiation field when there is no relative motion between the targets and a collective nuclear exciton is formed extending over both targets. This nuclear exciton is now disturbed by the sinusoidal US vibration. As shown in section 2, the periodic US motion can lead to nuclear exciton echoes.

4.1.1. Definite amplitude and definite initial phase

It is clear from section 2 and from figure 2 that all three types of echo effect can only be seen if two conditions are fulfilled:

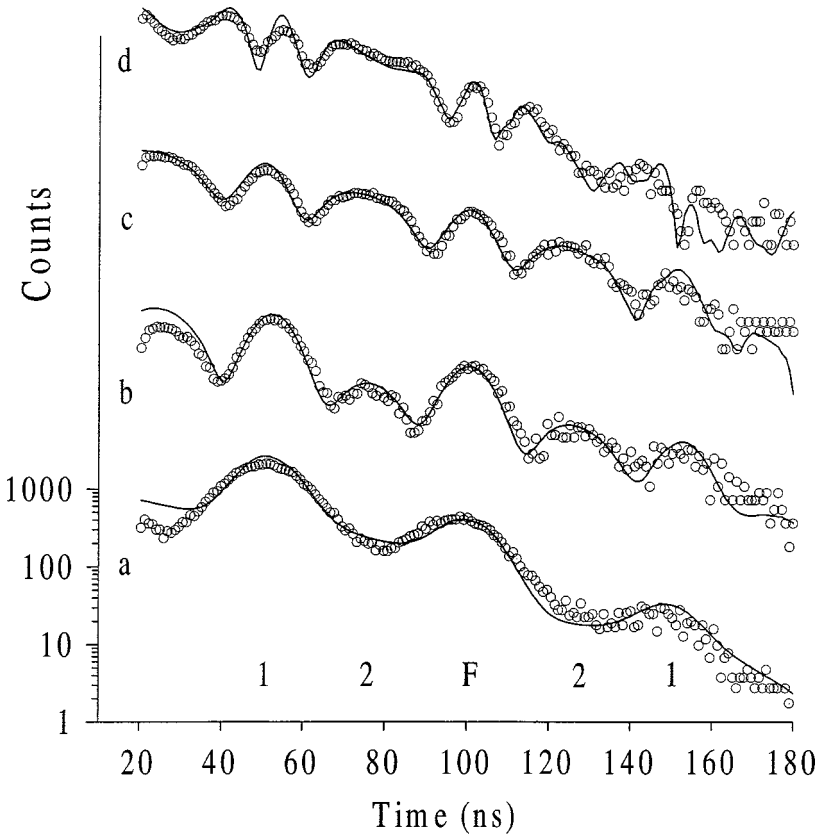

Figure 3. Three types of nuclear exciton echo observed with a piston-like US motion of a $\sim$ 1.35 μm SS foil mounted on a PVDF piezodriver. A second $\sim$ 1.35 μm SS foil was kept stationary. The US frequency was 9.94 MHz. The US vibration was phase-locked to the SR pulse. The initial phase Φ was kept constant at $\Phi = 0$. The US amplitude increases with US voltage from bottom to top. The corresponding modulation indices obtained from the fits are $w = 2.6$ (a), 4.4 (b), 5.3 (c), 8.4 (d). The curves are artificially shifted for a better display. The fundamental (F) echo as well as the intermediate echoes of the first (1) and second (2) kind are indicated. Here and in the figures below the solid curves are the fits with the dynamical theory (see text).

(a) the amplitude of vibration is homogeneous over the area of the foil, i.e., the motion is piston-like,

(b) the initial phase Φ is kept constant, i.e., the US motion is synchronized to the SR pulse.

Piston-like motion with definite amplitudes can be achieved by the use of a PVDF foil as a piezodriver. Φ can be kept constant by a phase-locked-loop circuit (see section 3.3). Figure 3 shows the results of such an experiment [11].

The solid lines are fits according to eq. (2.23) using the dynamical theory. All types of echoes, the fundamental one, and those of the 1st and 2nd kind, appear in the spectra. In contrast to the fundamental echoes and those of the 1st kind, which exist

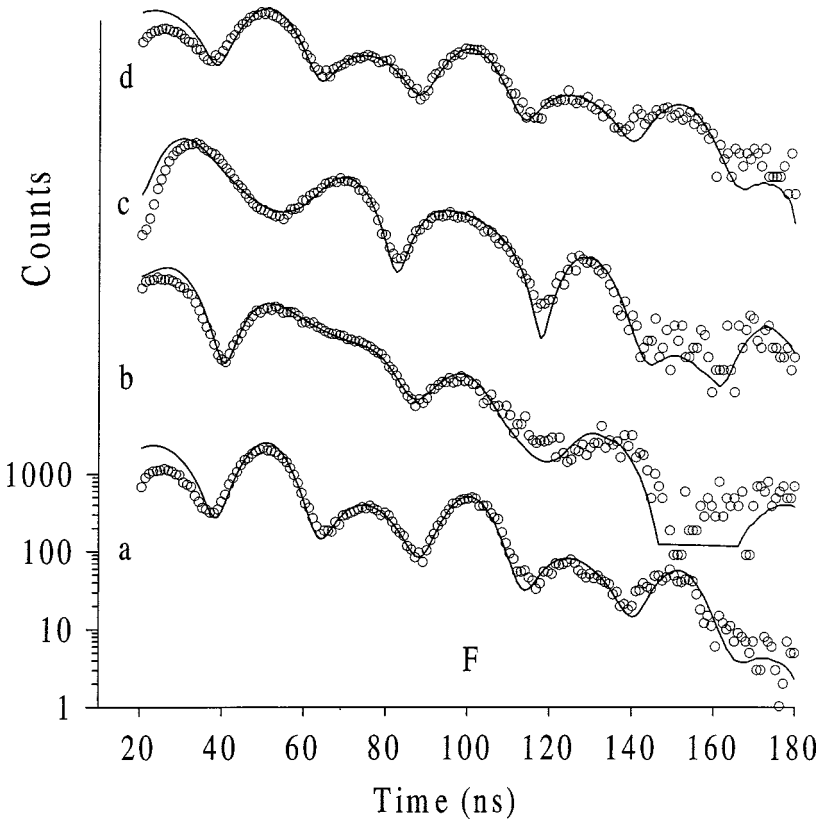

Figure 4. Three types of nuclear exciton echo observed at constant US amplitude for various values of the initial phase: $\Phi = 0$ (a); $\pi/4$ (b); $\pi/2$ (c); π (d). The fit gave a modulation index of $w = 4.4$. Other experimental details as in figure 3.

at all US amplitudes, echoes of the 2nd kind grow gradually with increasing rf voltage and are finally formed at the very top curve, where the amplitude of the US motion reaches $a \geqslant \lambda$ (compare with figure 2).

All echoes become sharper with increasing US vibration amplitude because of growing US motion velocity $|(\mathrm{d}/\mathrm{d}t)u(t)|$ at the positions of the echoes, so that the passage through the constructive interference range is faster.

Figure 4 displays results for the case where the rf voltage (i.e., the vibration amplitude) is kept constant; the initial phase, however, has been adjusted between 0 and π. The solid lines are again fits according to eq. (2.23).

The fundamental echoes are always present at the full period. However, their duration is not changed monotonously as in the previous case. This is because $(\mathrm{d}/\mathrm{d}t)u(t)$ is a sinusoidal function of Φ. For instance, when the echo position coincides with zero velocity, as in the case of $\Phi = \pi/2$, the echo reaches its maximum duration. For the intermediate echoes, their appearance in time is strongly dependent on the initial phase Φ, as follows from eq. (2.29) and figure 2 (see section 2).

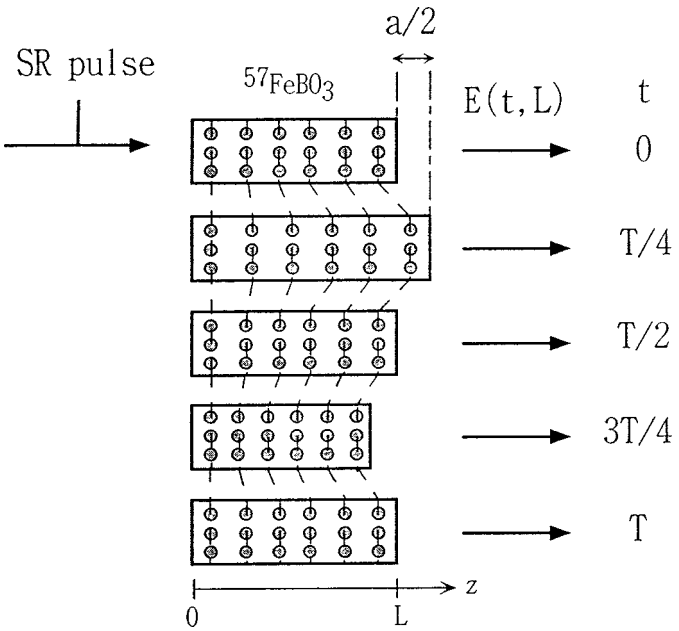

Figure 5. Magnetoelastic vibration of a $^{57}FeBO_3$ single crystal along the X-ray beam path. After a half rf period (at $t = T/2$) the nuclei have returned to their initial positions.

4.1.2. Definite initial phase, averaging over amplitudes

We now relax the condition of a definite vibration amplitude and only keep a constant initial phase with respect to the SR pulse. As an example of such an experiment we discuss the results of nuclear forward scattering (NFS) of SR by a magnetoelastically vibrated $^{57}FeBO_3$ single crystal. Figure 5 depicts the model assumed to describe the vibrations of the resonant nuclei. Figure 6 shows the time dependences observed [9,10].

In figure 6(a) only the static magnetic field was applied. Figure 6(b) was recorded in the presence of both the static and the rf modulation field. The rf field was phase-locked to the SR pulse. The initial phase was adjusted in such a way that the zero-crossing of the rf field coincided with the arrival of the SR pulse. Thus at $t = 0$, the direction of the magnetization of the crystal is parallel to the static magnetic field and – as in figure 6(a) – only the transitions with $\Delta m = 0$ are excited that give rise to a characteristic quantum beat (QB). A comparison of figures 6(a) and 6(b) shows that the period of the QB is not affected by the rf field, whereas the intensity distribution is drastically changed. In figure 6(b), the intensity in the time range between 25 and 160 ns is reduced, in contrast to the intensity enhancement around 210 ns.

The dashed lines in figure 6 represent calculated time spectra based on the dynamical theory. Speaking more qualitatively, the initial exciton formed at the incidence of the SR pulse at $t = 0$ and extending over the whole sample is disrupted at times $t > 0$ because of the vibration of the resonant nuclei. Dephasing of the γ-ray waves re-emitted from the individual nuclear layers leads to destructive interference by which

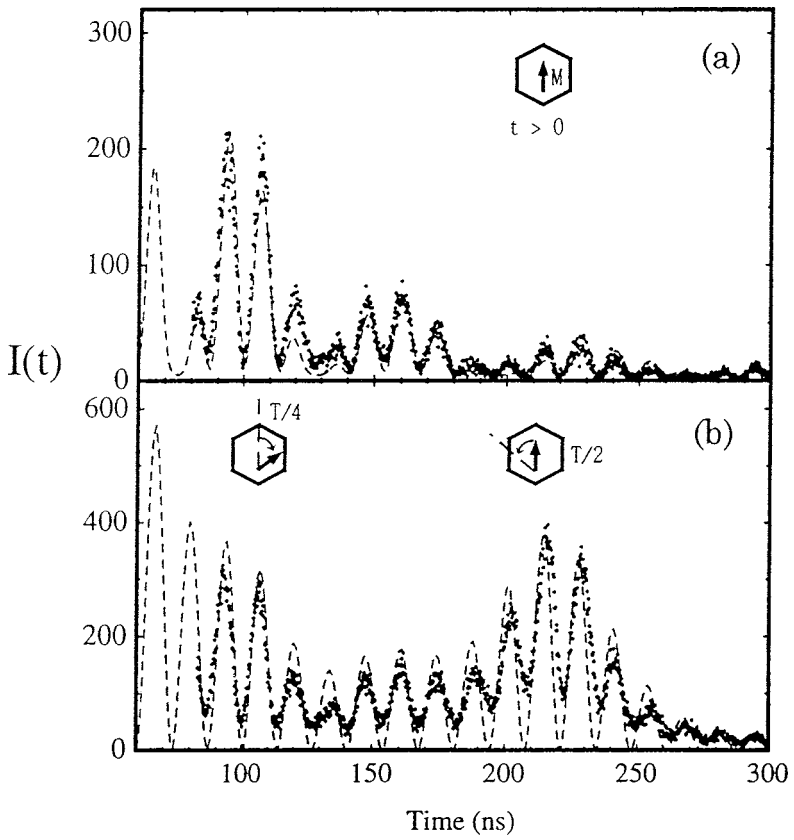

Figure 6. Time spectra of nuclear forward scattering from a $^{57}FeBO_3$ crystal. The magnetic field applied to the $^{57}FeBO_3$ crystal is (a) only the static magnetic field of 10 Oe, or (b) both the static magnetic field of 10 Oe and the rf magnetic field with an amplitude of 15 Oe and a frequency of 2.384 MHz. In case (b), the SR pulse is incident at the time of zero rf amplitude. The dashed lines represent calculated time spectra based on the dynamical theory.

the intensity of NFS decreases. However, rephasing is accomplished after half a period of the rf field when the magnetization of the crystal has been restored to its initial direction and as a consequence the resonant nuclei have returned to their initial positions (see figure 5). At this time, at $\sim$210 ns after the SR pulse, rephasing manifests itself in an echo-like increase of the NFS intensity. This is an echo of the 1st kind in accordance with our terminology.

A noteworthy aspect of this experiment is that echo-type phenomena can be observed by using one target only. This is possible because the nuclei are in layers at different depths, moving with respect to each other. Hence with respect to the motional state the crystal actually behaves like a "multilayered (multicomponent) target". As depicted in figure 5 the nuclear layers move in a breathing mode where the amplitudes vary between zero and a maximal value at the front and back crystal surfaces, respectively. Thus the averaging over the vibration amplitudes occurs along the direction

of the incoming radiation. Due to the averaging the amplitude-dependent echoes, i.e., those of the 2nd kind, are washed out and only the fundamental echoes and those of the 1st kind remain.

One should distinguish "longitudinal" averaging of the vibration amplitudes like in this case from the "transversal" one which is described in the next subsection. In the case of longitudinal averaging the *nuclear response amplitude* should be averaged while in the case of transversal averaging the *response intensity* is averaged over the vibration amplitude because the zones of piston-like vibration usually essentially exceed the size of the transverse coherence (Fresnel) zone.

4.1.3. Averaging over amplitudes and initial phase

Now we also relax the second condition and describe experiments where averaging occurs over amplitudes and the initial phase of the US vibration. Averaging over amplitudes can be achieved almost automatically by quartz drivers operated close to their thickness resonance frequencies. In this case averaging takes place over the target area, perpendicular to the direction of the incoming radiation. This is called "transversal" averaging. We consider again the situation of two targets (A and B) placed downstream behind each other.

(a) Two targets of the same thickness. This kind of experiment in fact led to the first observation of a nuclear exciton echo [3].

Figure 7 depicts the characteristic time dependencies for foils A and B together, both foils at rest (a), for foil A alone (b), and for foils A and B together where foil B is vibrated by US (c and d). For the case of an unperturbed system of the two foils the dynamical beat of the coherent emission characteristic for a nuclear exciton in a 2 μm target is observed (figure 7a). In contrast, the overall shape of the coherent emission from the perturbed (A + B) target (figures 7d, c) is close to the emission from a 1 μm foil (figure 7b). This result clearly proves that disruption of the whole nuclear exciton into two equivalent parts occurs in the case of US perturbation. However, at the times corresponding to multiples of the US period, pronounced increases of the forward scattered intensity are observed due to echo phenomena.

Figure 8 shows the evolution of the echo with increasing US vibration amplitude. The echo is at first very broad, becomes narrower with increasing US voltage, and becomes a sharp spike with a half-width of only ∼3 ns and a peak intensity twice the off-peak level. The solid lines in figures 7 and 8 are calculations using eq. (2.26) of the dynamical theory (see section 2).

Figures 7 and 8 show that only the fundamental echoes remain when averaging over both amplitude and phase. This can easily be understood from eq. (2.29) and from figure 2. At the moment of the excitation by the SR pulse and at multiples of the US period, $t_n = 2\pi n/\Omega$, the relative phase $\Psi(0) = 0$ (see section 2), the interference of emissions from the two targets in the forward direction is constructive, i.e., the maximum coherent emission characteristic for the total thickness of the combined

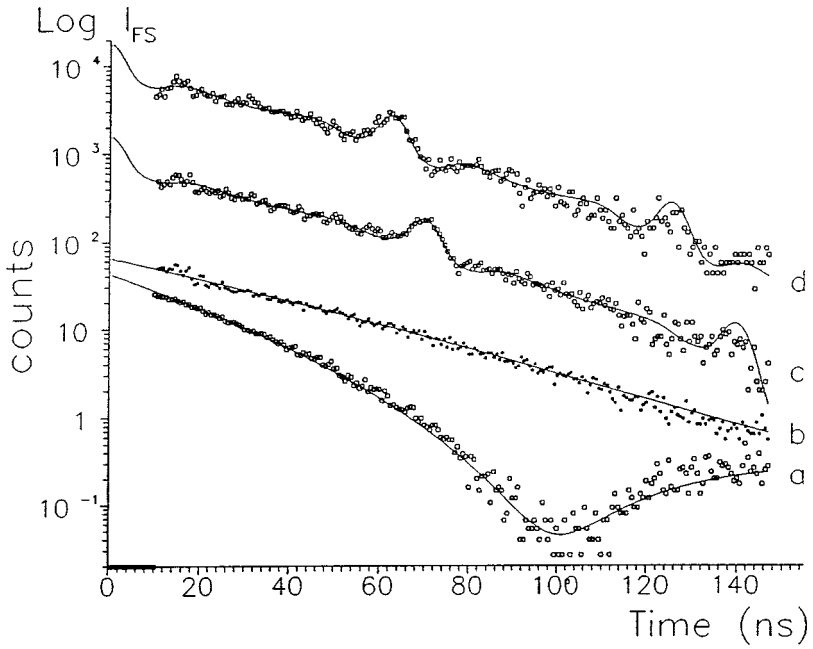

Figure 7. Time dependencies of nuclear forward scattering from two SS foils (A, B) for various conditions. The US excitation was applied to a $\sim$ 1 μm SS foil (foil A) mounted on a quartz piezodriver which was operated at different frequencies Ω and driving voltages U. (a) foils A + B, no vibration ($U = 0$); (b) foil A alone, no vibration ($U = 0$); (c) foils A + B, $\Omega/(2\pi) = 14.45$ MHz, $U = 5$ V; (d) foils A + B, $\Omega/(2\pi) = 16.0$ MHz, $U = 35$ V. The data sets are artificially shifted for a better display.

target (A + B) occurs, no matter what particular values hold for the amplitude and phase of the US vibration. However, at intermediate times the interference term in eq. (2.29) becomes zero due to averaging over the vibration amplitude (given by the index w) and over the phase Φ, and therefore the effect of the coherent emission from the combined target disappears.

Averaging over w and initial phase Φ is a crucial process in this experiment. From figures 2 and 4 (see above), and from eqs. (2.28) and (2.29) it is obvious that the positions of the intermediate echoes strongly depend on both w and Φ. Averaging over amplitude washes out echoes of the 2nd kind, while averaging over the phase washes out both echoes of the 1st and the 2nd kind, so that only the fundamental echoes remain. The time dependence of the emission at intermediate times is characteristic for the 1 μm target.

Thus the decay which starts at $t = 0$ with the coherent intensity of the combined targets ($T_A + T_B$) drops down after the disruption of the whole exciton by approximately a factor of 2 to the level of the incoherent sum of the emissions from targets A and B (compare figures 7a and 7c). The intensity decreases more slowly and shows no DB minimum at 100 ns. Only after each period, the coherent emission from both targets A and B can be seen, because the nuclear exciton extending over both foils is

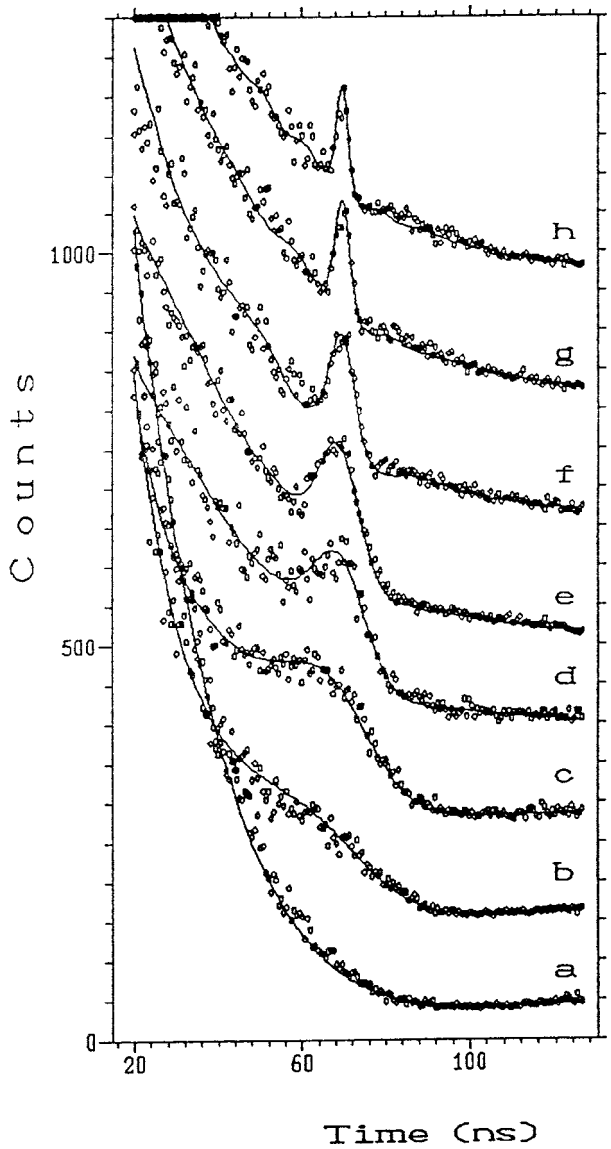

Figure 8. Evolution of the nuclear exciton echo with increasing US vibration amplitude. The US vibration was applied to foil A by a quartz piezodriver at $\Omega/(2\pi) = 14.45$ MHz and various driving voltages U. The corresponding modulation indices w were obtained from fits which are represented by the solid lines and are based on the dynamical theory. (a) $U = 0$ V, $w = 0$; (b) $U = 0.5$ V, $w = 0.6$; (c) $U = 1$ V, $w = 1.0$; (d) $U = 2$ V, $w = 2.0$; (e) $U = 3$ V, $w = 2.6$; (f) $U = 5$ V, $w = 4.4$; (g) $U = 8$ V, $w = 7.0$; (h) $U = 10$ V, $w = 8.8$. Other details as in figure 7.

reestablished and the emissions from both targets A and B are in phase again, leading to sharp total emission peaks. The speed of transition between the coherent and incoherent intensity levels increases with US amplitude. This effect is documented in figure 8.

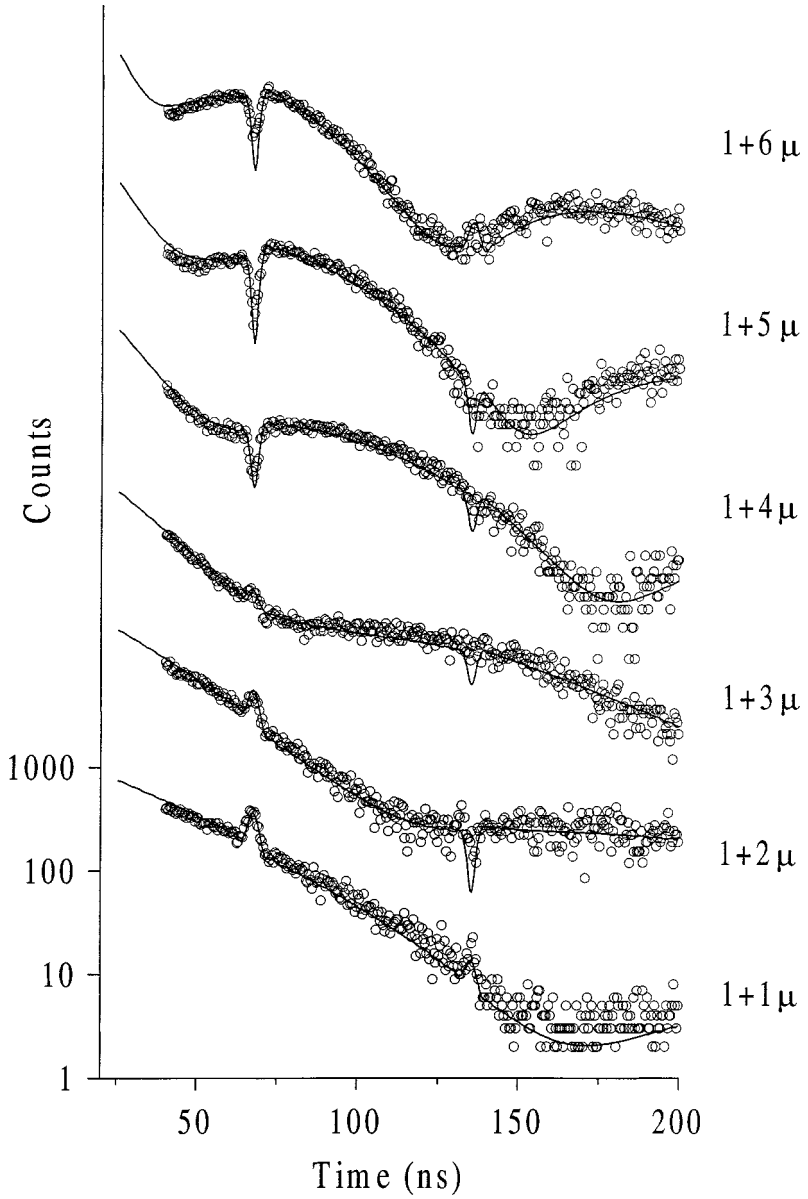

Figure 9. Nuclear exciton echoes obtained from a US vibrated SS foil of ~ 1 μm thickness in combination with stationary SS foils of various thicknesses. The US vibrations were generated by a quartz driver at $\Omega/(2\pi) = 14.54$ MHz. The curves are artificially shifted for a better display.

(b) Two targets with different thickness. An interesting modification arises when targets A and B have different thickness, all other experimental conditions being kept the same. Figure 9 shows experimental results obtained with a ~ 1 μm target, vibrated at 14.54 MHz by a quartz driver, and second targets of various thicknesses kept sta-

tionary [12]. Depending on the thickness of the second target not only echo peaks but also pronounced dips are observed at the times of the US period.

The solid lines represent calculations using eq. (2.26). A qualitative explanation is similar to that given in section (a) above. If the US vibrations lead to an efficient radiative de-coupling of the targets the initial nuclear exciton extending over both targets (A + B) is disrupted soon after $t = 0$. The two excitons formed in the separate targets develop almost independently and, because of the different target thicknesses, differently with time. The emissions from the targets are summed coherently but their interference results in quite different patterns in different scattering events because an individual scattering event is specified by a stochastic initial phase and amplitude of the US motion within the permitted distribution. Due to averaging over these parameters of the US motion the interference effect is washed out. However, at the times around $t_n = 2\pi n/\Omega$, where the relative phase $\Psi(t_n) = 0$, the interference effect can be observed again and again, exhibiting the effect of multiple echoes. The result of the interference around the times t_n depends on the amplitudes and phases of the interfering wave packets.

The radiation field emerging from each target (A, B) is modulated by envelopes $A(\tau)_{\mathrm{A,B}}$, where $A(\tau)_{\mathrm{A,B}} \propto (T\sigma)_{\mathrm{A,B}} = \{TJ_1(\sqrt{T\tau})/\sqrt{T\tau}\}_{\mathrm{A,B}}$. Since the Mössbauer thickness T is different for both targets, the corresponding envelopes $A(\tau)$ will also differ. In particular, because of the Bessel function J_1 the envelope $A(\tau)$ exhibits a slow oscillatory behavior and can also become negative. This in fact means the inversion of the phase of the γ-ray oscillation (carrier oscillation). For identical targets both envelopes have the same sign, i.e., the carrier oscillations are in phase at all t_n. Thus at all t_n only intensity peaks develop. However, for targets with different thicknesses not only the amplitude but also the phase of the carrier oscillations in the interfering wave packets may be different at t_n. In particular, when the oscillations are in anti-phase, dips in intensity instead of peaks will develop as observed in figure 9. Thus this technique provides a rather straightforward method to probe the amplitude and the phase of a wave packet [13,14].

An elegant modification of this technique is described in [15]: Both targets A and B are kept stationary. Between target A and target B a non-resonant coherent scatterer is placed. In [15] an X-cut quartz single crystal adjusted at the Bragg angle of the $(1, 1, -2, 0)$ reflection was used. Target B and avalanche detector were put into the reflected beam. The quartz single crystal was again vibrated in its thickness mode. In this way the radiation transmitted through target A is phase modulated by the vibration of the quartz crystal. This procedure is fully equivalent to the one described above where target A was vibrated by a quartz driver. Figure 10 gives examples for various combinations of target thicknesses where – similar to figure 9 above – echo peaks and dips were observed.

Since the target does not have to be glued to the vibrator, also very thin, high-frequency quartz crystals can be employed. In addition, this method provides the possibility to investigate the “vibrator”, which does not have to contain Mössbauer isotopes and which by no means always has to be a solid. For example, this method

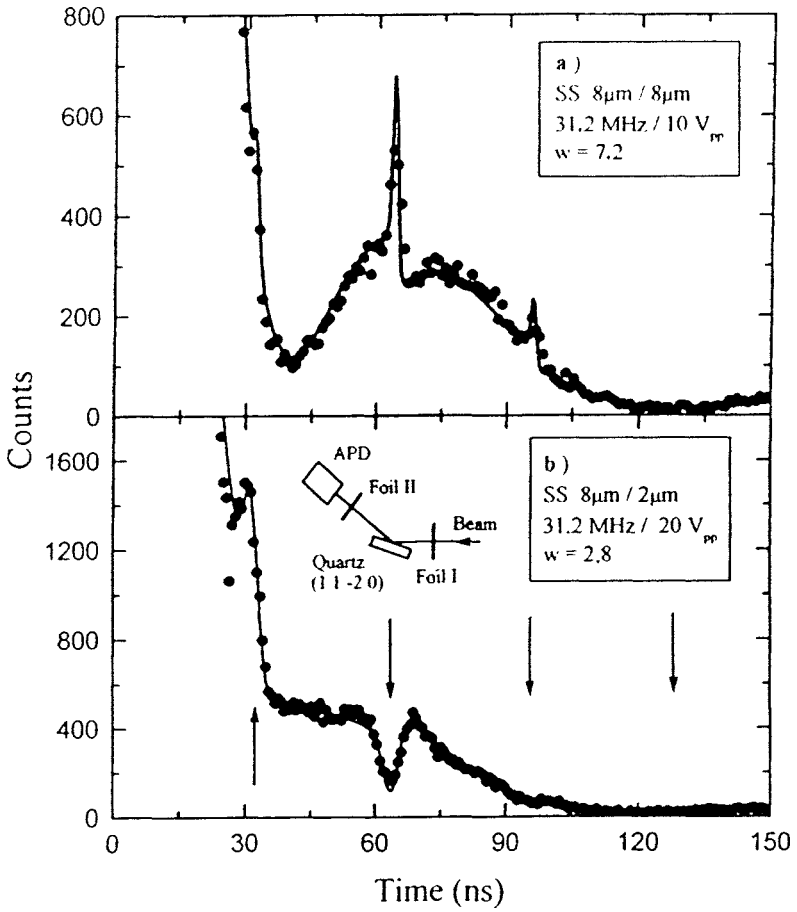

Figure 10. Nuclear exciton echoes observed with two SS foils, both of 8 μm thickness (a) and of 8 μm and 2 μm thicknesses (b). The expected US echoes are marked by arrows in (b). Experimental conditions concerning the US vibration are given in the insets.

allows the study of quasi-elastic coherent scattering of diffusive motions in liquids [16].

4.2. Vanishing coupling between the targets

In all experiments discussed in section 4.1 above, the initial nuclear exciton was perturbed by the US vibration of the resonant nuclei. Due to the relative motion of the targets the radiative coupling between them was disrupted and dephasing of their emissions occurred. Because of the periodical character of the motion, however, at certain times the coupling was re-established and the initial phasing of the emissions was recovered (in case of equally thick targets). Both the re-establishment of the radiative coupling and the rephasing led to echo-like phenomena in the form of drastic changes

of the forward scattering intensity due to the coherent response of the whole target at these times.

Obviously, if the radiative coupling between the two targets were suppressed at all times, the scattering from the combined target could be reduced to the case where only the two-path interference process is important. This situation can be realized by moving one of the targets at a certain Doppler velocity, for example at a constant velocity v, relative to the second target. When the velocity is large enough, i.e., $(v/c)\omega_0 \gg \Gamma$, there is practically no radiative coupling between the two targets. In this case the excitons created by the SR pulse in targets A and B develop independently and since the emissions from targets A and B are coherent, the interference of the individual A and B emissions can be observed.

Let us consider the effect of an additional US excitation of one of the targets under these conditions. The delayed part of the wave packet transmitted through both targets is given by eq. (2.25). Again, the relative phase $\Psi(t)$ between the radiation fields from targets A and B is given by the exponent:

$$\Psi(t) = \Delta\omega t + w\big\{\sin[\Omega t + \Phi] - \sin\Phi\big\}.$$

The relative phase is now composed of two parts: the "running" phase $\Psi^{(1)}(t)$ that is increasing with time at a constant rate $\Psi^{(1)}(t) \propto \Delta\omega t = (v/c)\omega_0 t$ and the oscillating phase $\Psi^{(2)}(t) = w\{\sin[\Omega t + \Phi] - \sin\Phi\}$, which is oscillating with the US frequency Ω within the limited range $(2\pi a/\lambda)$.

The effect of $\Psi^{(1)}(t)$ alone is well known as the quantum beat (QB) of the forward scattering intensity. The effect of $\Psi^{(2)}(t)$ is the nuclear exciton echo phenomenon discussed in detail above. In the following we shall see that echo-type phenomena still arise when $\Psi(t) = \Psi^{(1)}(t) + \Psi^{(2)}(t)$, i.e., both the US vibration and a constant velocity are applied.

Figure 11 displays results of an experiment where target A was US vibrated by a quartz crystal and at the same time target B was moved at a constant Doppler velocity v by a conventional double-loudspeaker drive. Neither motion was synchronized to the SR pulse [17].

The solid lines represent fits according to eq. (2.27). The lowest curve in figure 11 shows the time dependence when no US motion is applied. The initial nuclear exciton is immediately disrupted by the constant velocity motion. Both targets are totally decoupled. The cosine function of eq. (2.27) describes a QB, the frequency of which is given by

$$\frac{\mathrm{d}\Psi(t)}{\mathrm{d}t} = \Delta\omega = \frac{v}{c}\omega_0 = \text{const.}$$

and is thus determined by the Doppler velocity v. The QB pattern at $t = 0$ always starts close to its maximum. This can be seen from eq. (2.27), where for $t = 0$ in the cosine function only the thickness term $T_{\mathrm{AB}}/[4(\Delta\omega + n\Omega)t_0]$ remains. If $\Delta\omega$ is large, this term is close to zero and the cosine exhibits nearly its maximal value. When the US motion is switched on the QB structure vanishes with increas-

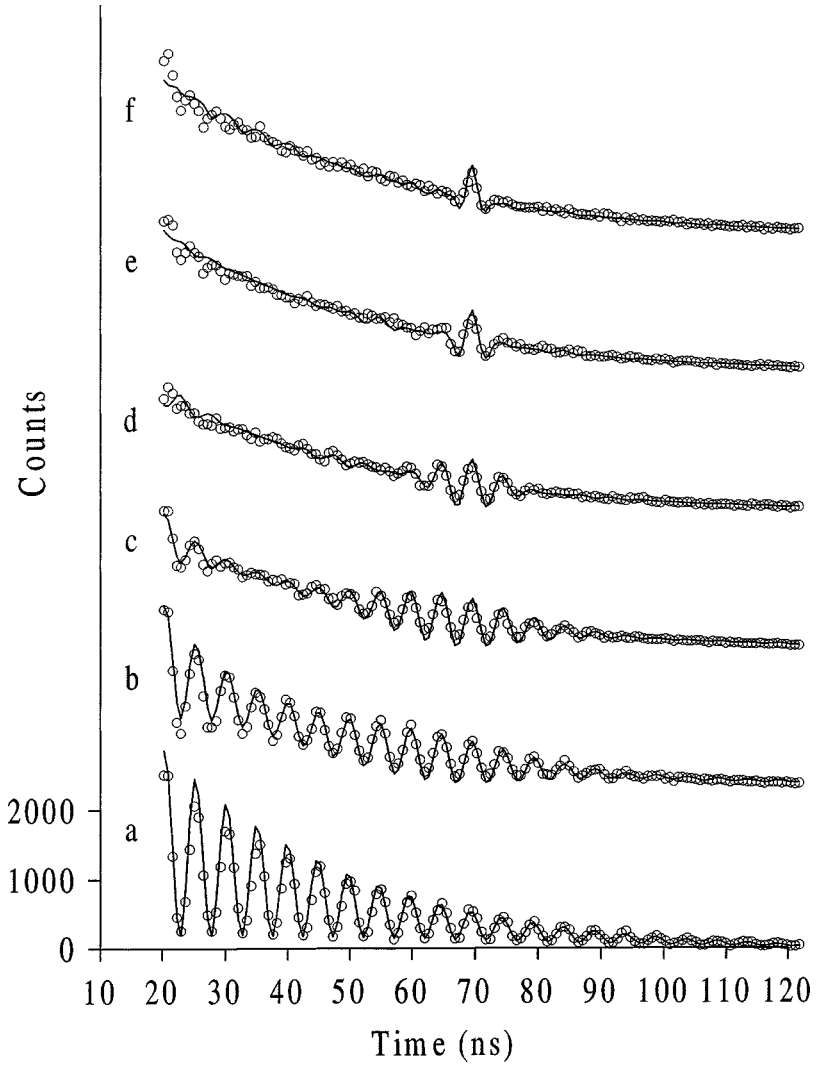

Figure 11. Inter-resonance interference between nuclei of target A and of target B moved at a constant velocity of ± 18 mm/s with respect to target A. In addition, target A is US vibrated by a quartz driver operated at $\Omega/(2\pi) = 14.54$ MHz and various US voltages. The US amplitude increases with US voltage U from bottom to top. The corresponding modulation indices w were obtained from the fits. (a) $U = 0$ V, $w = 0$; (b) $U = 1$ V, $w = 0.9$; (c) $U = 1.5$ V, $w = 1.2$; (d) $U = 2.5$ V, $w = 2.6$; (e) $U = 5$ V, $w = 5.6$; (f) $U = 9.8$ V, $w = 9.8$. Neither motion is synchronized to the SR pulse. The QB interference pattern is washed out with increasing US voltage (US amplitude) except for the time region around the full US period (69 ns).

ing US amplitude and is finally completely washed out except for the time regions around the full US period P (at 69 ns). This effect can be compared to the narrowing of the width of the echo as shown in figure 8. However, the washout of the QB structure in figure 11 provides a very pronounced visualization of the influence

of an increasing US amplitude (modulation index) on the forward scattering intensity.

The US motion gives an additional oscillating contribution to $\Psi(t)$. Therefore, as mentioned in section 2, eq. (2.31), $\mathrm{d}\Psi(t)/\mathrm{d}t$ is no longer constant, and as a result the QB turns out to be frequency modulated, the maximal frequency deviation, i.e., the modulation index, being proportional to the US amplitude. Since the US motion is not synchronized to the SR pulse the frequency modulation effectively contributes to the washout of the QB except at the time P. Here the phase of the US motion is the same as at $t = 0$ where the SR pulse occurs. Since $t = 0$ is characterized by constructive interference, the same holds at time P. The larger the US amplitude (modulation index), the shorter in time is the region around P which survives the washout. This picture is fully supported by eq. (2.27). If the US amplitude is small the summation over $n = 0, \pm 1$ is sufficient. Then only the frequencies $\Delta\omega, \Delta\omega + \Omega$, and $\Delta\omega - \Omega$ are involved. This leads to a washout of QB beyond the time interval $\Delta t \approx (2\Omega)^{-1}$ around the maxima (see figure 11, curve b). At higher US amplitudes, larger values of n are involved, leading to a more rapid washout of the QB as shown in the upper curves of figure 11. Calculations show that also the averaging process over the US amplitudes contributes significantly to the washout of the QB pattern.

Interesting phenomena are predicted by eq. (2.28), which can be applied to experiments where the phase of the US motion is locked to the SR pulse. The most exciting aspect is that now the QB is predicted to be frequency modulated by US. As mentioned in section 2, eq. (2.31), $\Delta\omega_i = \Delta\omega + w\Omega\cos(\Omega t + \Phi)$, i.e., the frequency of the QB varies between $\Delta\omega - w\Omega$ and $\Delta\omega + w\Omega$, depending on the modulation index (amplitude) of the US motion. Such measurements, where the US motion is synchronized with the SR pulse and definite amplitudes are achieved by PVDF drivers, are in progress.

5. Summary

The application of US to an excited nuclear ensemble causes a perturbation of the nuclear excitation delocalized over the ensemble, i.e., of the nuclear exciton. Particularly, in combination with physically separated targets it is a very effective method for the investigation of nuclear excitons. If a periodic US vibration is used the nuclear exciton extending initially over the whole system of targets can not only be perturbed in a controllable fashion, but it can be restored periodically, exhibiting collective coherent emissions: nuclear exciton echoes. When the modulation index w (amplitude a) of the US motion is small, both the interference term and the coupling term determine the coherent emission in the forward direction.

When $w\Omega = ka\Omega > \Gamma$, i.e., the maximum velocity of the US motion is large, the nuclear exciton is disrupted into two parts which hardly communicate via the radiation field, i.e., are radiatively decoupled. The emission from the whole system is then well presented by the interference of the emissions from the separate parts. The result of

interference is strongly determined by the phasing of the constituent wave packets. Due to the periodical character of the motion, systematic dephasing and rephasing of the wave packets takes place, leading to the periodical variation of the coherent forward emission with time.

Different possibilities should be distinguished depending on the experimental conditions:

(a) The phase correlation between the wave packets is preserved for the full decay time and is repeated identically during each scattering event. This case is realized for a piston-like US vibration synchronized with the SR pulses. The time dependence of the forward scattering intensity in this case is determined by the interference (constructive, destructive and so on) of the constituting wave packets during the whole observation time.

(b) The phase correlation of the wave packets holds within each scattering event for the whole time but changes from event to event except for those times that are multiples of the US period, $t_n = 2\pi n/\Omega$. This is the case when the US motion is not synchronized with the SR pulses and is *inhomogeneous over the area of the target* which is US vibrated. Then *averaging the scattering intensity* over w and Φ washes out the interference effect for almost all times except for the time intervals in the vicinity of t_n, where the interference of the wave packets is preserved and leads to echo phenomena: peaks or dips of the scattering intensity.

(c) At each instant of one scattering event except for certain time intervals there is a phase distribution between the constituent forward scattered wavelets. An example is a breathing vibration mode of one target. In such a mode the *physical thickness* of the target changes because of the relative motion of the nuclear planes along the beam path. However, the motion of the nuclei is *inhomogeneous*. Even though the vibration is synchronized with the SR pulses one has to *average the wavefield amplitude* over the vibration amplitude in this case, which results in the disappearance of coherent scattering. However, at times around $t_n/2$ all vibration amplitudes become zero in this type of motion and the constituent forward-scattered wavelets are added constructively, yielding peaks of the forward-scattered intensity – echoes of the nuclear exciton. In the absence of synchronization the echoes would appear only at times around t_n.

When the nuclear exciton is disrupted by applying a constant-velocity Doppler motion to a separate target, interference of the emissions from the targets is the dominant mechanism. If in addition one target is US vibrated, the inter-resonance interference, taking place in this case, leads not only to echo-like phenomena but also to a frequency modulation of the quantum beats. All experimental results are quantitatively described by the dynamical theory.

6. Acknowledgements

This work has been supported by the Bundesministerium für Bildung, Wissenschaft, Forschung und Technologie under Contract No. 643WOA and by INTAS-RFBR under Contract No. 95-0586. The authors would like to thank Dr. U. van Bürck, Dr. S.L. Popov, and P. Schindelmann, for many stimulating discussions and critical reading of the manuscript.

Appendix

For the evaluation of the integral

$$S_n = \frac{1}{2\pi}\int_{-\infty}^{+\infty} \mathrm{d}\omega \cdot \mathrm{e}^{\mathrm{i}\omega t}\, \mathrm{e}^{\mathrm{i}\frac{T_A/2}{2(\omega-\omega_0)t_0-\mathrm{i}}}\, \mathrm{e}^{\mathrm{i}\frac{T_\mathrm{B}/2}{2(\omega-\omega_0-n\Omega)t_0-\mathrm{i}}} \tag{A.1}$$

we assume $t_0\Omega \gg 1$, which corresponds to our experimental conditions. This assumption will allow us to find an analytical solution for the integral:

We set $v = 2(\omega-\omega_0)t_0 - \mathrm{i}$ and rewrite the integral:

$$S_n = \frac{1}{2\pi}\int_{-\infty}^{+\infty} \mathrm{d}\omega \cdot \mathrm{e}^{\mathrm{i}\omega t}\, \mathrm{e}^{\mathrm{i}\frac{T_\mathrm{A}/2}{v}}\, \mathrm{e}^{\mathrm{i}\frac{T_\mathrm{B}/2}{v-2n\Omega t_0}}. \tag{A.2}$$

We expand the second and third exponentials in the integrand into Taylor series and write eq. (A.2) as the sum of the following four integrals:

$$\begin{aligned} S_n = {} & \frac{1}{2\pi}\int_{-\infty}^{+\infty} \mathrm{d}\omega \cdot \mathrm{e}^{\mathrm{i}\omega t} + \frac{1}{2\pi}\int_{-\infty}^{+\infty} \mathrm{d}\omega \cdot \mathrm{e}^{\mathrm{i}\omega t} \sum_{k=1}^{\infty} \frac{1}{k!}\left(\mathrm{i}\frac{T_\mathrm{A}/2}{v}\right)^k \\ & + \frac{1}{2\pi}\int_{-\infty}^{+\infty} \mathrm{d}\omega \cdot \mathrm{e}^{\mathrm{i}\omega t} \sum_{m=1}^{\infty} \frac{1}{m!}\left(\mathrm{i}\frac{T_\mathrm{B}/2}{v-2n\Omega t_0}\right)^m \\ & + \frac{1}{2\pi}\int_{-\infty}^{+\infty} \mathrm{d}\omega \cdot \mathrm{e}^{\mathrm{i}\omega t} \sum_{k=1}^{\infty} \frac{1}{k!}\left(\mathrm{i}\frac{T_\mathrm{A}/2}{v}\right)^k \sum_{m=1}^{\infty} \frac{1}{m!}\left(\mathrm{i}\frac{T_\mathrm{B}/2}{v-2n\Omega t_0}\right)^m. \end{aligned} \tag{A.3}$$

The first integral in eq. (A.3) yields the well known Dirac δ-function, so that the first term in eq. (A.3) represents the prompt part of the transmitted wave packet

$$I^{(1)} = \delta(t). \tag{A.4}$$

We rewrite the second term in eq. (A.3) using the v-axis for integration. Taking into account that

$$\omega = \frac{1}{2t_0}(v+\mathrm{i}) + \omega_0$$

we obtain

$$I^{(2)} = \frac{1}{2\pi}\,\frac{1}{2t_0}\,\mathrm{e}^{\mathrm{i}\omega_0 t-\tau/2}\int_{-\infty-\mathrm{i}}^{+\infty-\mathrm{i}} \mathrm{d}v \cdot \mathrm{e}^{\mathrm{i}v\tau/2} \sum_{k=1}^{\infty} \frac{1}{k!}\left(\mathrm{i}\frac{T_\mathrm{A}}{2v}\right)^k. \tag{A.5}$$

The integration axis now lies in the complex v-plane. For a while we omit the pre-integral factor and evaluate the integral itself. We expand the first exponential into its Taylor series as well and thus present the whole integrand as a power series of v:

$$\int_{-\infty-\mathrm{i}}^{+\infty-\mathrm{i}} \mathrm{d}v \cdot \sum_{l=0}^{\infty} \frac{1}{l!}\left(\mathrm{i}v\frac{\tau}{2}\right)^{l} \sum_{k=1}^{\infty} \frac{1}{k!}\left(\mathrm{i}\frac{T}{2v}\right)^{k}. \tag{A.6}$$

We have so far omitted the label at the effective thickness T. For evaluation of this integral we complete the contour on the semi-circle in the upper part of the complex v-plane and apply the residue theorem for executing the integration

$$\oint_{v=0} \mathrm{d}v \cdot F(v) = 2\pi\mathrm{i}\,\mathrm{Res}\,\big[F(v)\big]. \tag{A.7}$$

The residue of the integrand can be found as the coefficient of the term containing v^{-1} in the product of sums in eq. (A.6). We write explicitly the sums in $F(v)$

$$\left[1 + \mathrm{i}\frac{v\tau}{2} - \frac{1}{2!}\left(\frac{v\tau}{2}\right)^{2} - \mathrm{i}\frac{1}{3!}\left(\frac{v\tau}{2}\right)^{3} + \cdots\right]$$
$$\times \left[\mathrm{i}\frac{T}{2v} - \frac{1}{2!}\left(\frac{T}{2v}\right)^{2} - \mathrm{i}\frac{1}{3!}\left(\frac{T}{2v}\right)^{3} + \frac{1}{4!}\left(\frac{T}{2v}\right)^{4} + \cdots\right]$$

and readily find the coefficient at v^{-1}:

$$\mathrm{Res}\big[F(v)\big] = \mathrm{i}\frac{T}{2} - \mathrm{i}\frac{1}{2!}\,\frac{T}{2}\,\frac{T\tau}{4} + \mathrm{i}\frac{1}{2!}\,\frac{1}{3!}\,\frac{T}{2}\left(\frac{T\tau}{4}\right)^{2} - \cdots \tag{A.8}$$

or

$$\mathrm{Res}\big[F(v)\big] = \mathrm{i}\frac{T}{2}\sum_{M=0}^{\infty} \frac{1}{M!(M+1)!}\left(-\frac{T\tau}{4}\right)^{M}. \tag{A.9}$$

In this form the residue closely fits the following power series expansion of the Bessel function of real argument and first order:

$$J_1(x) = \frac{x}{2}\sum_{M=0}^{\infty} \frac{1}{M!(M+1)!}\left(-\frac{x^2}{4}\right)^{M}. \tag{A.10}$$

We set $x = \sqrt{T\tau}$ and now the residue can be expressed via the Bessel function

$$\mathrm{Res}\big[F(v)\big] = \mathrm{i}\sqrt{\frac{T}{\tau}}\,J_1\big(\sqrt{T\tau}\big). \tag{A.11}$$

Substituting eq. (A.11) into eq. (A.7) and eq. (A.7) into eq. (A.5) we obtain the following result for the second integral:

$$I^{(2)} = -\frac{1}{2t_0}\,\mathrm{e}^{\mathrm{i}\omega_0 t - \tau/2}\sqrt{\frac{T_\mathrm{A}}{\tau}}\,J_1\big(\sqrt{T_\mathrm{A}\tau}\,\big), \tag{A.12}$$

where the label at T has been restored. Making use of the σ-function (introduced in eqs. (2.10) and (2.17)) we have

$$I^{(2)} = -\frac{1}{2t_0}\,\mathrm{e}^{\mathrm{i}\omega_0 t-\tau/2}(T\sigma)_{\mathrm{A}}. \tag{A.13}$$

For the evaluation of the third integral we use the new variable $v' = v - 2n\Omega t_0$. Then

$$\omega = \frac{1}{2t_0}\big(v' + \mathrm{i}\big) + \omega_0 + n\Omega.$$

We thus arrive at the same integral as given by eq. (A.5) with the additional phase factor exp(i$n\Omega t$). So the result can be immediately written as

$$I^{(3)} = -\frac{1}{2t_0}\,\mathrm{e}^{\mathrm{i}(\omega_0+n\Omega)t-\tau/2}(T\sigma)_{\mathrm{B}}. \tag{A.14}$$

As to the fourth integral, the integrand there has the two well distant poles at $v = 0$ and at $v_1 = 2n\Omega t_0$, with $n \neq 0$. Therefore the solution for this integral can be searched for in the following way:

$$I^{(4)} = 2\pi\mathrm{i}\big[\mathrm{Res}(v) + \mathrm{Res}(v_1)\big]. \tag{A.15}$$

While finding the first residue we use the identity

$$\sum_{m=1}^{\infty}\frac{1}{m!}\left(-\mathrm{i}\frac{T_{\mathrm{B}}}{4n\Omega t_0}\right)^m = \mathrm{e}^{-\mathrm{i}\frac{T_{\mathrm{B}}}{4n\Omega t_0}} - 1$$

and arrive at

$$2\pi\mathrm{i}\,\mathrm{Res}(v) = -\frac{1}{2t_0}\,\mathrm{e}^{\mathrm{i}\omega_0 t-\tau/2}(T\sigma)_{\mathrm{A}}\Big[\mathrm{e}^{-\mathrm{i}\frac{T_{\mathrm{B}}}{4n\Omega t_0}} - 1\Big]. \tag{A.16}$$

The second residue is found in a similar way:

$$2\pi\mathrm{i}\,\mathrm{Res}(v_1) = -\frac{1}{2t_0}\,\mathrm{e}^{\mathrm{i}(\omega_0+n\Omega)t-\tau/2}(T\sigma)_{\mathrm{B}}\Big[\mathrm{e}^{\mathrm{i}\frac{T_{\mathrm{A}}}{4n\Omega t_0}} - 1\Big]. \tag{A.17}$$

Substituting the solutions given by eqs. (A.4), (A.13)–(A.17) into eq. (A.3) we finally obtain

$$S_n = \delta(t) - \frac{1}{2t_0}\,\mathrm{e}^{\mathrm{i}\omega_0 t-\tau/2}\Big[\mathrm{e}^{-\mathrm{i}\frac{T_{\mathrm{B}}}{4n\Omega t_0}}(T\sigma)_{\mathrm{A}} + \mathrm{e}^{\mathrm{i}n\Omega t}\,\mathrm{e}^{\mathrm{i}\frac{T_{\mathrm{A}}}{4n\Omega t_0}}(T\sigma)_{\mathrm{B}}\Big]. \tag{A.18}$$

References

[1] G.V. Smirnov, this issue, section II-2.

[2] Yu. Kagan, A.M. Afanas'ev and V.G. Kohn, J. Phys. C 12 (1979) 615.

[3] G.V. Smirnov, U. van Bürck, J. Arthur, S.L. Popov, A.Q.R. Baron, A.I. Chumakov, S.L. Ruby, W. Potzel and G.S. Brown, Phys. Rev. Lett. 77 (1996) 183.

[4] Yu.V. Shvyd'ko, A.I. Chumakov, G.V. Smirnov, V.G. Kohn, T. Hertrich, U. van Bürck, E. Gerdau, H.D. Rüter, J. Metge and O. Leupold, Europhys. Lett. 22 (1993) 305.

[5] V.G. Kohn and Yu.V. Schvyd'ko, J. Phys. Condens. Matter 7 (1995) 7589.
[6] G.V. Smirnov, Hyp. Int. 97/98 (1996) 551.
[7] H. Ohigashi, J. Appl. Phys. 47 (1976) 949.
[8] The foils were kindly provided by Stan Ruby.
[9] T. Mitsui, T. Shimizu, Y. Imai, Y. Yoda, X.W. Zhang, H. Takei, T. Harami and S. Kikuta, Jpn. J. Appl. Phys. 36 (1997) 6525.
[10] S. Kikuta, Y. Yoda, I. Koyama, T. Shimizu, H. Igarashi, K. Izumi, Y. Kunimune, M. Seto, T. Mitsui, T. Harami, X. Zhang and M. Ando, in: *X-Ray and Inner-Shell Processes*, AIP, Vol. 389 (1997) 351.
[11] U. van Bürck, G.V. Smirnov and J. Arthur, ESRF Report HS-122 (1997).
[12] G.V. Smirnov, S.L. Popov, U. van Bürck, W. Potzel, P. Schindelmann, E. Gerdau, O. Leupold, Yu.V. Shvyd'ko and H.D. Rüter, HASYLAB Annual Report Part I, 890 (1996).
[13] G.V. Smirnov, U. van Bürck, W. Potzel, S.L. Popov, P.S. Schindelmann, E. Gerdau, O. Leupold, Yu.V. Shvyd'ko and H.D. Rüter, in: *ICAME 97*, Book of Abstracts, MO.T15.P06.
[14] U. van Bürck, W. Potzel, P. Schindelmann, G.V. Smirnov, S.L. Popov, E. Gerdau, O. Leupold, Yu.V. Shvyd'ko and H.D. Rüter, HASYLAB Annual Report Part I, 884 (1996).
[15] H. Jex, A. Ludwig, F.J. Hartmann, E. Gerdau and O. Leupold, Europhys. Lett. 40 (1997) 317; A. Ludwig and H. Jex, Physica B 254 (1998) 1.
[16] A.Q.R. Baron, H. Franz, A. Meyer, R. Rüffer, A.I. Chumakov, E. Burkel and W. Petry, Phys. Rev. Lett. 79 (1997) 2823.
[17] U. van Bürck, W. Potzel, P. Schindelmann, G.V. Smirnov, S.L. Popov, E. Gerdau, O. Leupold, Yu.V. Shvyd'ko and H.D. Rüter, HASYLAB Annual Report Part I, 888 (1996).